for the dynamic morphological changes of spermatids. Understanding this process and identifying the molecular factors involved in IMT have been interesting targets for research. There are a number of reports examining IMT and these two vesicle transport systems in conditions other than spermiogenesis. Molecular motors on the microtubule track, such as kinesin [33, 34] and cytoplasmic dynein [35], are found in testis and in the manchettes of other species. The expression of kinesin-II was confirmed in rat spermatid tail [33]. Kinesin, a heterotetramer, consists of two heavy chains and two light chains (KLCs). The heavy chains contain a catalytic domain necessary for ATP hydrolysis and microtubule binding. KLCs might function in cargo binding or in the regulation of kinesin activity. Mice encode three KLC isoforms, KLC1, KLC2, and KLC3. KLC3, which is expressed in round and elongating spermatids, is observed in sperm tails, suggesting a specialized function in this location [34]. Cytoplasmic dynein is reported to be associated with manchette microtubules spermiogenesis in rat [35]. The signal for cytoplasmic dynein in rats corresponded well with the expression pattern of the manchette in step 7–10 spermatids in humans and monkeys. In intraflagellar transport, which uses the molecular motors kinesin and dynein and the same kind of microtubule-based vesicle transport system as IMT, simultaneous genetic knockout of the two kinesin-II motor subunits completely abrogated the formation of cilia in *Tetrahymena* [36]. Removal of the gene encoding one of the subunits of kinesin-II, *KIF3A*, by Cre-loxP mutagenesis from mouse photoreceptor cells resulted in extensive apoptotic death of photoreceptor cells [37]. Vesicles in these cells, such as those containing opsin, accumulated within the inner segment, suggesting that those materials could not be transported to the outer segment along the connecting cilium.

Myosin Va, the molecular motor on the F-actin track, is associated with the manchette and manchette-associated vesicles within rat spermatids [21]. To our knowledge, however, there is little additional evidence that actin-based vesicular transport participates in IMT. Actin-based vesicular transport has primarily been studied through melanosome transport. Rab GTPases regulate melanosome vesicle formation, docking, tethering, and fusion [18, 19]. Rab27a, a melanosomal membrane protein, recruits myosin Va to the melanosome surface through a rabphilin-like effector protein, melanophilin [15]. In melanosomes, myosin Va binds indirectly to Rab27a through Slac2-a/melanophilin, a synaptotagmin-like protein homolog lacking the C2 domain-a: [14]. Slac2-c, a homolog of Slac2-a, interacts with Rab27a/b and myosin Va/VIIa; this protein is highly expressed in the brain, lung, and testis [17]. MyRIP, which has structural similarities to Slac2-a/melanophilin, interacts with both Rab27a and myosin VIIa and is associated with melanosomes [16]. Griscelli syndrome, a human genetic disease, and the corresponding mouse model, *ashen* [38], result from a defect in the Rab27a gene [18]. Patients have partial albinism of hair and skin resulting from the failure of melanosome transport to keratinocytes.

Which cargo proteins are transported by IMT during spermiogenesis? There are several possibilities. 1) Cargo proteins might be transported to the developing sperm tail by IMT for tail formation. This idea is supported by a number of reports detailing that keratins, including *Sak57* [6], Odf1 [39, 40], and Odf2 [41], keratin-associated proteins, such as Spag4 [42] and Spag5 [43], the 26S proteasome [4, 7], *N*-arginine convertase [44], an RNA-binding protein [45], and type 4 cAMP-specific phosphodiesterase [46] are transiently stored in the manchette. *Sak57*, Odf1, Odf2, and the 26S proteasome are sorted to the outer dense fibers of the tail, whereas *N*-arginine convertase is sorted to the axoneme. 2) Cargo proteins necessary for spermatid nuclear condensation are transported by IMT. This idea is supported by a report describing the presence of Ran, a Ras-related GTPase, in the cytoplasm and nucleus of round spermatids and in the manchettes of elongating spermatids. Ran GTPase is thought to control the trafficking of nuclear proteins during the spermatid nuclear condensation [47]. The manchette might play a role in trimming the residual spermatid cytoplasm. By pulling the cytoplasm down to the distal side, residual cytoplasm can be discarded during spermiation [48]. Unnecessary materials in the cytoplasm could be transported to the distal side through the microtubule or F-actin tracks in IMT.

In conclusion, this study suggested that, during primate spermiogenesis, the manchette contains the molecular motor dynein on a microtubule track, and the molecular motor myosin Va, the motor recruiter MyRIP, and the vesicle receptor Rab27b on an F-actin track. We speculated that these factors that compose microtubule-based and actin-based vesicle transport systems might actually be involved in IMT. In particular, this is the first report regarding expression of these factors in the

manchette during primate spermiogenesis.

Acknowledgment

We are grateful to Dr Mitsunori Fukuda (Tohoku university, Sendai, Japan) for his kind advice and to Dr Masakuni Suzuki (Suzuki Memorial Hospital, Miyagi, Japan).

References

1 Clermont Y, Oko R, Hermo L. Cell Biology of Mammalian Spermatogenesis. In: Desjardins C, Ewing LL, editors. Cell and Molecular Biology of the Testis. New York: Oxford University Press; 1993: p332–76.
2 Meistrich ML. Nuclear morphogenesis during spermiogenesis. In: de Kretser D, editor. Molecular Biology of the Male Reproductive System. New York: Academic Press; 1993: p67–97.
3 Cole A, Meistrich ML, Cherry LM, Trostle-Weige PK. Nuclear and manchette development in spermatids of normal and *azh/azh* mutant mice. Biol Reprod 1988; 38: 385–401.
4 Mochida K, Tres LL, Kierszenbaum AL. Structural and biochemical features of fractionated spermatid manchettes and sperm axonemes of the *azh/azh* mutant mice. Mol Reprod Dev 1999; 52: 434–44.
5 Kierszenbaum AL, Tres LL. Bypassing natural sperm selection during fertilization: the *azh* mutant offspring experience and the alternative of spermiogenesis *in vitro*. Mol Cell Endocrinol 2002; 187: 133–8.
6 Tres LL, Kierszenbaum AL. Sak57, an acidic keratin initially present in the spermatid manchette before becoming a component of paraaxonemal structures of the developing tail. Mol Reprod Dev 1996; 44: 395–407.
7 Rivkin E, Cullinan EB, Tres LL, Kierszenbaum AL. A protein associated with the manchette during rat spermiogenesis is encoded by a gene of the TBP-1-like subfamily with highly conserved ATPase and protease domains. Mol Reprod Dev 1997; 47: 77–89.
8 Kierszenbaum AL. Spermatid manchette: plugging proteins to zero into the sperm tail. Mol Reprod Dev 2001; 59: 347–9.
9 Kierszenbaum AL. Intramanchette transport (IMT): managing the making of the spermatid head, centrosome, and tail. Mol Reprod Dev 2002; 63: 1–4.
10 Kierszenbaum AL, Tres LL. The acrosome–acroplaxome–manchette complex and the shaping of the spermatid head. Arch Histol Cytol 2004; 67: 271–84.
11 Kierszenbaum AL, Tres LL, Rivkin E, Kang-Decker N, Van Deursen JM. The acroplaxome is the docking site of Golgi-derived myosin Va/Rab 27a/b-containing proacrosomal vesicles in wild-type and Hrb mutant mouse spermatids. Biol Reprod 2004; 70: 1400–10.
12 Stamnes M. Regulating the actin cytoskeleton during vesicular transport. Curr Opin Cell Biol 2002; 14: 428–33.
13 Rosenbaum JL, Witman GB. Intraflagellar transport. Nat Rev Mol Cell Biol 2002; 3: 813–25.
14 Wu XS, Rao K, Zhang H, Wang F, Sellers JR, Matesic LE, *et al.* Identification of an organelle receptor for myosin-Va. Nat Cell Biol 2002; 4: 271–8.
15 Langford GM. Myosin-V, a versatile motor for short-range vesicle transport. Traffic 2002; 3: 859–65.
16 El-Amraoui A, Schonn JS, Kussel-Andermann P, Blanchard S, Desnos C, Henry JP, *et al.* MyRIP, a novel Rab effector, enables myosin VIIa recruitment to retinal melanosome. EMBO Rep 2002; 3: 463–70.
17 Fukuda M, Kuroda TS. Slac2-c (synaptotagmin-like protein homologue lacking C2 domain-C), a novel linker protein that interacts with Rab27, myosin Va/VIIa, and actin. J Biol Chem 2002; 277: 43096–103.
18 Seabra MC, Mules EH, Hume AN. Rab GTPase, intracellular traffic and disease. Trends Molec Med 2002; 8: 23–30.
19 Goud B. How Rab proteins link motors to membranes. Nat Cell Biol 2002; 4: E77–78.
20 Goode BL, Drubin DG, Barnes G. Functional cooperation between the microtubule and actin cytoskeleton. Curr Opin Cell Biol 2000; 12: 63–71.
21 Kierszenbaum AL, Rivkin E, Tres LL. The actin-based motor myosin Va is a component of the acroplaxome, an acrosome-nuclear envelop junctional plate, and of manchette-associated vesicles. Cytogenet Genome Res 2003; 103: 337–44.
22 Mochida K, Tres LL, Kierszenbaum AL. Isolation of the rat spermatid manchette and its perinuclear ring. Dev Biol 1998; 200: 46–56.
23 Johnsen SG. Testicular biopsy score count--a method for registration of spermatogenesis in human testes: normal values and results in 335 hypogonadal males. Hormones 1970; 1: 2–25.
24 Manandhar G, Moreno RD, Simerly C, Toshimori K, Schatten G. Contractile apparatus of the normal and abortive cytokinetic cells during mouse male meiosis. J Cell Sci 2000; 113: 4275–86.
25 Clermont Y. The cycle of the seminiferous epithelium in man. Am J Anat 1963; 112: 35–51.
26 Heller GC, Clermont Y. Kinetics of the germinal epithelium in man. Recent Prog Horm Res 1964; 20: 545–75.
27 Johnson L, Neaves WB, Barnard JJ, Keillor GE, Brown SW, Yanagimachi R. A comparative morphological study of human germ cells *in vitro* or *in situ* within seminiferous tubules. Biol Reprod 1999; 61: 927–34.
28 Johnson L, Saub C, Neaves WB, Yanagimachi R. Live human germ cells in the context of their spermatogenic stages. Hum Reprod 2001; 16: 1575–82.
29 Clermont Y, Leblond CP. Spermiogenesis of man, monkey, ram and other mammals as shown by the periodic acid-Schiff technique. Am J Anat 1955; 96: 229–53.
30 Clermont Y, Leblond CP. Differentiation and renewal of spermatogonia in the monkey, *Macacus rhesus*. Am J Anat 1959; 104: 237–73.
31 Clermont Y. Two classes of spermatogonial stem cells in the monkey (*Cercopithecus aethiops*). Am J Anat 1969; 126: 57–72.
32 Chen D, Guo J, Miki T, Tachibana M, Gahl WA. Molecular cloning and characterization of rab 27a and 27b, novel human

rab proteins shared by melanocytes and platelets. Biochem Molec Med 1997; 60: 27–37.
33 Miller MG, Mulholand DJ, Vogl WA. Rat testis motor proteins associated with spermatid translocation (dynein) and spermatid flagella (kinesin-II). Biol Reprod 1999; 60: 1047–56.
34 Junco A, Bhullar B, Tarnasky HA, van der Hoorn FA. Kinesin light chain KLC3 expression in testis is restricted to spermatids. Biol Reprod 2001; 64: 1320–30.
35 Yoshida T, Ioshii SO, Imanaka-Yoshida K, Izutsu K. Association of cytoplasmic dynein with manchette microtubules and spermatid nuclear envelope during spermiogenesis in rats. J Cell Sci 1994; 107: 625–33.
36 Rosenbaum JL, Cole DG, Diener DR. Intraflagellar transport: the eyes have it. J Cell Biol 1999; 144: 385–8.
37 Marszalek JR, Liu XR, Roberts D, Chui JD, Marth DS, Williams DS, *et al.* Genetic evidence for selective transport of opsin and arrestin by kinesin-II in mammalian photoreceptors. Cell 2000; 102: 175–82.
38 Wilson SM, Yip R, Swing DA, O'Sullivan TN, Zhang Y, Novak EK, *et al.* A mutation in Rab27a causes the vesicle transport defects observed in *ashen* mouse. Proc Natl Acad Sci USA 2000; 97: 7933–8.
39 Van der Hoorn FA, Tarnasky HA, Nordeen SK. A new rat gene *RT17* is specially expressed during spermiogenesis. Dev Biol 1990; 143: 147–54.
40 Burfeind P, Hoyer-Fender S. Sequence and developmental expression of a mRNA encoding a putative protein of rat sperm outer dense fibers. Dev Biol 1991; 148: 195–204.
41 Brohmann H, Pinnecke S, Hoyer-Fender S. Identification and characterization of new cDNAs encoding outer dense fiber proteins of rat sperm. J Biol Chem 1997; 272: 10327–32.
42 Shao X, Tarnasky HA, Lee JP, Oko R, van der Hoorn FA. Spag4, a novel sperm protein, binds outer dense fiber protein Odf1 and localizes to microtubules of the manchette and axoneme. Dev Biol 1999; 211: 109–23.
43 Shao X, Xue J, van der Hoorn FA. Testicular protein Spag5 has similarity to mitotic spindle protein Deepest and binds outer dense fiber protein Odf1. Mol Reprod Dev 2001; 59: 410–6.
44 Chesneau V, Prat A, Segretain D, Hospital V, Dupaix A, Foulon T, *et al.* NRD convertase: a putative processing endoprotease associated with the axoneme and manchette in late spermatids. J Cell Sci 1996; 109: 2737–45.
45 Schumaker JM, Lee K, Edelhoff S, Braun RE. Spnr, a murine RNA binding protein that is located to cytoplasmic microtubules. J Cell Biol 1995; 129: 1023–32.
46 Salanova M, Chun SY, Iona S, Puri C, Stefanini M, Conti M. Type 4 cyclic adenosine monophosphate-specific phoshodiesterases are expressed in discrete subcellular compartments during rat spermiogenesis. Endocrinology 1999; 149: 2297–306.
47 Kierszenbaum AL, Gil M, Rivkin E, Tres LL. Ran, a GTP-binding protein involved in nucleocytoplasmic transport and microtubule nucleation, relocates from the manchette to the centrosome region during rat spermiogenesis. Mol Reprod Dev 2002; 63: 1–4.
48 Toshimori K, Ito C. Formation and organization of the mammalian sperm head. Arch Histol Cytol 2003; 66: 383–96.

Edited by Dr Will W. M. Lee

Laboratory Animals

Vet Pathol 45:67–72 (2008)

BRIEF COMMUNICATIONS and CASE REPORTS

Transthyretin Amyloidosis and Two Other Aging-Related Amyloidoses in an Aged Vervet Monkey

S. NAKAMURA, S. OKABAYASHI, N. AGEYAMA, H. KOIE, T. SANKAI, F. ONO, K. FUJIMOTO, AND K. TERAO

The Corporation for Production and Research of Laboratory Primates, Tsukuba, Ibaraki, Japan (SN, SO, FO, KF); Tsukuba Primate Research Center, National Institute of Biomedical Innovation, Tsukuba, Ibaraki, Japan (NA, TS, KT); and the Department of Veterinary Medicine, College of Bioscience, Nihon University, Fujisawa, Kanagawa, Japan (HK)

Abstract. An aged male vervet monkey showed severe cardiac arrhythmia for more than 3 years. A multifocal amyloid consisting of transthyretin was deposited in all areas of the heart wall, especially in the extracellular stroma among muscle fibers and external tunica of arterioles. Moreover, the amyloid was deposited in the stroma and arterioles of other systemic organs except the liver and spleen. These characteristics are consistent with senile systemic amyloidosis in humans. A second amyloid consisting of amyloid β protein was in senile plaques and cerebral amyloid angiopathy in the cerebral cortex. A third amyloid consisting of islet amyloid polypeptide was deposited in islets of the pancreas. Apolipoprotein E and amyloid P component colocalized with the 3 amyloids. Thus, 3 different aging-related amyloids were found in an aged vervet monkey. In particular, to our knowledge, this is the first report on spontaneous transthyretin amyloidosis in animals.

Key words: Amyloidosis; amyloid β protein; IAPP; transthyretin.

Amyloid is a degenerative protein that exhibits common biochemical and morphologic characteristics, such as 1) birefringence under polarizing microscope, 2) abundant β pleated–sheets in the secondary structure of the proteins, and 3) nonbranching and nonparallel straight fibrils (8–10 nm in diameter) under electron microscope.[13] However, each amyloid consists of different precursor proteins.[13] Furthermore, amyloidosis may develop secondary to various conditions, such as inflammation, aging, and certain neoplasms. Transthyretin (TTR), amyloid β protein (Aβ), and islet amyloid polypeptide (IAPP) amyloidoses are well known as major aging-related amyloidoses.[15] Among these amyloids, senile systemic amyloidosis (SSA), which is characterized by the deposition of amyloid fibrils containing TTR, is well known in aged humans but not in animals. In SSA, first small amyloid deposits, mainly in the heart, occur without obvious symptoms. However, in some case, massive amyloid deposits result in heart failure, eventually leading to death.[15]

In nonhuman primates, limited literature on amyloidosis is available. However, cerebral Aβ and islet amylin amyloidoses have been investigated in nonhuman primates as models for Alzheimer's disease and diabetes mellitus, respectively.[7,10] In the vervet monkey, there has only been one report on cerebral Aβ deposition preventable by Aβ vaccination,[4] whereas no study has been conducted for other types of amyloidoses.

A male vervet monkey (*Cercopithecus aethiops*), assumed to be 29 years old, showed severe cardiac arrhythmia for more than 3 years and bradycardia at the later stage of the 3 years, which were detected by 4-leads electrocardiography. Premature ventricular contractions (PVCs) were monitored by 24-hour Holter electrocardiography. The frequency of PVCs gradually became severe (3,000 PVCs per day) during the 3 years. Moreover, dilatation of the right ventricle was detected by ultrasound and X-ray examinations. However, for the left ventricle, no obvious disorders, such as reduced left ventricular ejection fractions, were observed by echocardiography. Symptoms associated with Alzheimer's disease and diabetes mellitus were not observed in the present case. Finally, the monkey was euthanized because of poor prognosis due to severe depression and anorexia.

At necropsy, collected tissues were fixed in 10% buffered formalin, embedded in paraffin, and sectioned at 4 μm. The deparaffinized sections were stained with hematoxylin and eosin. Some sections were stained with Congo red and direct fast scarlet (DFS; Muto, Tokyo,

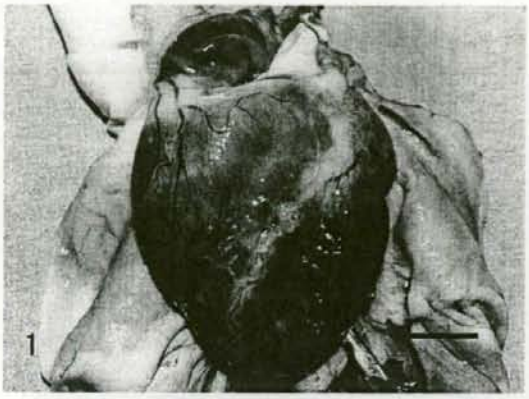

Fig. 1. Heart; Vervet monkey. Heart revealed slight dilatation with various sized pale white spots on the surface. Bar = 1 cm.

Japan) with or without potassium permanganate (PPM). Positive reactions for Congo red and DFS were confirmed by apple green birefringence under polarizing microscope. Furthermore, some deparaffinized sections were immunostained using rabbit polyclonal antibodies against Aβ 1–42 (Aβ42; Chemicon, Temecula, CA; 1:100), amyloid P component (AP; DAKO, Glostrup, Denmark; 1:300), apolipoprotein E (apoE; DAKO; 1:1000), calcitonin (IBL, Takasaki, Japan; 1:400), kappa light chains (κAL; DAKO; 1:20000), lambda light chains (λAL; DAKO; 1:40000), and TTR (DAKO; 1:100) and using mouse monoclonal antibodies against amyloid A (AA; Novocastra, Newcastle, UK; 1:100) and IAPP (Serotec, Raleigh, NC; 1:100). Sections immunostained for Aβ42 were pretreated with 99% formic acid for 10 minutes. The remaining immunostains used pretreatment with citrate buffer (pH 6.0, 121°C, 10 min). These sections were further reacted with horseradish peroxidase-conjugated secondary mouse and rabbit immunoglobulins (EnVision+ System, DAKO) and then visualized with 3,3′-diaminobenzidine tetrahydrochloride (DAB).

At necropsy, the heart revealed slight dilatation of both ventricles with thinning of the right ventricular free wall. The surface of the heart was reddish brown with pale white spots (Fig. 1). The brain and pancreas showed slight atrophy.

Myocardium and stroma were multifocally replaced by hyaline material deposits, mainly in the free wall of the ventricles (Fig. 2). Hyaline deposits were observed regardless of the area in the heart, such as subendocardium or subepicardium and right or left wall. They showed uniform pale pink staining with hematoxylin and eosin in the extracellular stroma among the heart muscle fibers (Fig. 3). These hyaline deposits were positive for DFS and Congo red (Fig. 4, Table 1), and their reactions were resistant to PPM (data not shown). DFS and Congo red stained the hyaline deposits; however, DFS showed less nonspecific background than did Congo red. Apple green birefringence corresponding to their hyaline deposits was observed by both DFS and Congo red under polarizing microscope (data not shown). The intensity of birefringence was stronger with Congo red than with DFS (data not shown). Moreover, in the heart, DFS- and Congo red–positive deposits were observed in the external tunica of some arterioles. These cardiac amyloids were immunohistochemically positive for antibodies against TTR, apoE, and AP (Fig. 5, Table 1). The intensity of TTR immunoreactivity was most significant. Moreover, immunoreactivity of TTR as well as of apoE was greater than that of AP. Heart muscle fibers adjoining the amyloid lesions showed necrotic or atrophic changes (Fig. 3).

Hyaline deposits were found mainly in the stromal connective tissues (fibrous and adipose tissues) and external tunic of the blood vessels. Moreover, faint deposits were observed in the peripheral nerves of the thyroid gland, tonsil, salivary glands, thymus, prostate gland, lymph nodes, and skeletal muscles (Table 1). As for mucosal organs, the deposits were found in lamina propria of the tongue, trachea, esophagus, stomach, intestines, and urinary bladder; submucosal layers of the stomach and intestines; muscular layer of the intestines and urinary bladder; and serosa of the trachea and esophagus (Table 1). Furthermore, hyaline deposits in the lungs were found in the alveolar walls, bronchial wall, and external tunica of arterioles (Table 1). In the kidneys, the deposits were detected in the renal pelvis and external tunica of the arcuate arteries (Table 1). In these organs, severe deposits were found in the thyroid gland, tongue, esophagus, and stomach; moderate deposits in the tonsil, thymus, lungs, intestines, and skeletal muscles; and weak deposits in the salivary glands, trachea, kidneys, urinary bladder, and lymph nodes. These deposits were positive for DFS and Congo red (Table 1) but resistant to PPM and revealed apple green birefringence under polarizing microscope (data not shown). These were immunohistochemically positive for antibodies against TTR, apoE, and AP (Table 1). The intensity of immunoreactivity was stronger for TTR and apoE than for AP. Furthermore, TTR-positive but DFS- and Congo red–negative lesions were detected in the external tunica of blood vessels of the testes. Reactivity for DFS and Congo red and immunoreactivity of TTR, apoE, and AP were not detected in the liver, spleen, pituitary, and adrenal gland (Table 1). Thus, based on histochemical and immunohistochemical characteristics of cardiac and other amyloids, systemic amyloidosis characterized by the deposition of amyloid fibrils containing TTR was confirmed.

The second type of hyaline deposit, such as neuritic senile plaques (SPs), was observed in the cerebral cortices. DFS and Congo red detected not only some neuritic SPs but also deposits consistent with cerebral amyloid angiopathy (CAA) (Table 1), as found previously in vervet and cynomolgus monkeys.[4,5] This type of amyloid was resistant to PPM and revealed apple green birefringence under polarizing microscope (data

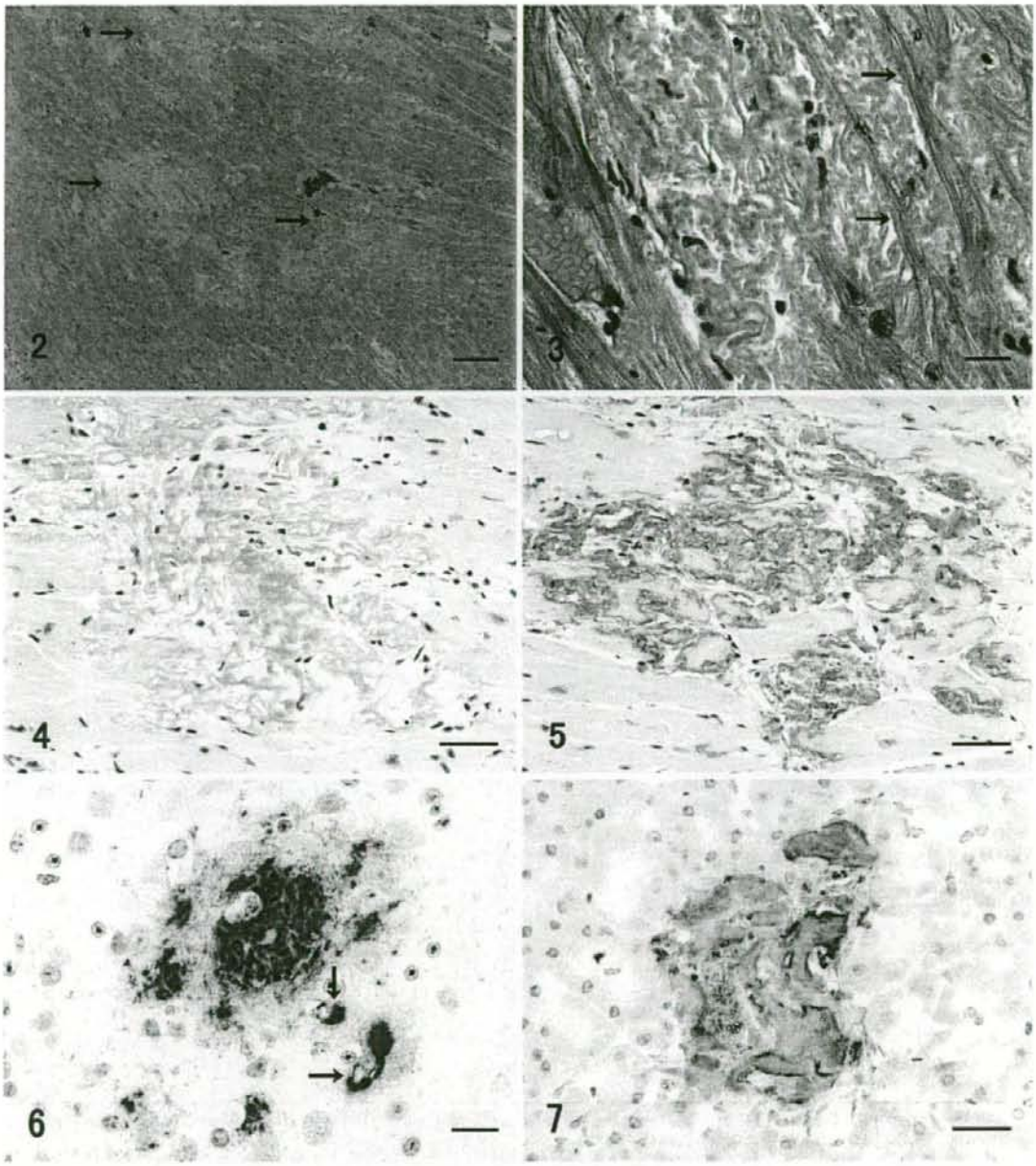

Fig. 2. Heart; vervet monkey. Hyaline deposits (arrows) were multifocally found in the heart wall. HE. Bar = 200 μm.

Fig. 3. Heart; vervet monkey. Hyaline materials showed uniform pale pink staining, and the surrounding muscle fibers revealed atrophic and necrotic changes (arrows). HE. Bar = 20 μm.

Fig. 4. Heart; vervet monkey. Hyaline materials were positive for direct fast scarlet (DFS). DFS. Bar = 50 μm.

Fig. 5. Heart; vervet monkey. Amyloid deposits were immunohistochemically positive for antibodies against transthyretin. Immunoperoxidase method, hematoxylin counterstain. Bar = 50 μm.

Fig. 6. Cerebrum; vervet monkey. Cerebral amyloid deposits, such as neuritic senile plaques and capillary-cerebral amyloid angiopathy (arrows), were immunohistochemically positive for antibodies against amyloid β protein. Immunoperoxidase method, hematoxylin counterstain. Bar = 20 μm.

Fig. 7. Pancreas; vervet monkey. Islet amyloid deposits were immunohistochemically positive for antibodies against islet amyloid polypeptide (IAPP). Immunoperoxidase method, hematoxylin counterstain. Bar = 20 μm.

Table 1. Histochemical and immunohistochemical features of amyloid depositions in various organs and tissues of an aged vervet monkey.

Organ or Tissue	DFS*	Congo Red	TTR	Aβ	IAPP	apoE	AP	Notes
Brain	++	+	−	+++	−	++	+	Senile plaques and amyloid angiopathy
Pituitary	−	−	−	−	−	−	−	
Thyroid	+++	++	+++	−	−	+++	+++	Parafollicular areas
Parathyroid	−	−	−	−	−	−	−	
Tongue	+++	+++	+++	−	−	+++	+++	Tunica propria, stroma, and blood vessels
Tonsil	++	+	++	−	−	+++	++	Stroma and adjoining connective tissues
Salivary	+	+	+	−	−	+	+	Stroma, blood vessels, and adjoining connective tissues
Trachea	+	+	++	−	−	+	+	Tunica propria and serosa
Esophagus	+++	+++	+++	−	−	+++	+++	Tunica propria, muscle layer, and serosa
Heart	+++	+++	+++	−	−	+++	+++	Myocardium and blood vessels
Thymus	++	++	+++	−	−	+++	++	Stroma and adjoining connective tissues
Lungs	++	++	+++	−	−	+++	+++	Alveolar and bronchus walls and blood vessels
Stomach	+++	+++	+++	−	−	+++	++	Tunica propria, submucosal and muscle layer, and blood vessels
Intestines	++	++	+++	−	−	+++	++	Tunica propria, muscle layer, and blood vessels
Pancreas	++	++	−	−	+++	+++	++	Islets
Liver	−	−	−	−	−	−	−	
Gall bladder	−	−	−	−	−	−	−	
Spleen	−	−	−	−	−	−	−	
Kidneys	+	+	+	−	−	+	+	Renal pelvis and arcuate arteries
Adrenal	−	−	−	−	−	−	−	
Testes	−	−	+	−	−	−	−	Blood vessels
Prostate	+++	+++	+++	−	−	+++	+++	Stroma and blood vessels
Urinary bladder	+	+	+	−	−	+	+	Muscle layer and blood vessels
Lymph nodes	+	+	++	−	−	++	+	Stroma, blood vessels, and adjoining connective tissues
Skeletal muscle	++	++	++	−	−	++	+	Stroma and blood vessels
Sciatic nerve	−	−	−	−	−	−	−	
Bone	−	−	−	−	−	−	−	
Bone marrow	−	−	−	−	−	−	−	
Skin	NT	NT	NT	NT	NT	NT	NT	

*DFS = direct fast scarlet; TTR = transthyretin; Aβ = amyloid β protein; IAPP = islet amyloid polypeptide; apoE = apolipoprotein E; AP = amyloid P component.

+++ = strong positive; ++ = moderate positive; + = weak positive; − = negative; NT = not tested.

not shown). Furthermore, SPs and CAA were immunohistochemically labeled using antibodies against Aβ42, apoE, and AP (Fig. 6, Table 1). The intensity of immunoreactivity was stronger with Aβ42 and apoE than with AP. Diffuse plaques, found previously in cynomolgus monkeys,[5] were not found in the present case. This amyloid derived from Aβ was not deposited in the other organs (Table 1).

The third type of hyaline deposit was found in the expanded stromal areas of islets of the pancreas. This was positive for Congo red and DFS and resistant to PPM (Table 1) and showed apple green birefringence under polarizing microscope (data not shown). This amyloid was immunohistochemically positive for antibodies against IAPP, apoE, and AP (Fig. 7, Table 1). The intensity of immunoreactivity was stronger with

IAPP and apoE than with AP. The islets, where abundant amyloid was deposited, had a reduced number of islet cells. This IAPP-derived amyloid was not detected from any other organ (Table 1).

Finally, all the 3 types of hyaline deposits were immunohistochemically negative for antibodies against AA, calcitonin, κAL, and λAL (Table 1).

Although there is no information about amino acid sequences of TTR, Aβ, and IAPP in vervet monkeys, the sequences in human are 93.1%, 100%, and 94.6% homology (BAC20609 and XP_001098180),[11] respectively, against those in macaque monkeys and vervet monkeys, who belong taxonomically to *Cercopithecus*. Antibodies to TTR and Aβ used in the present study have reacted with each amyloid lesion, that is, cardiac amyloid in SSA and SPs in AD, consisting of intact mature amyloid in human.[8,12] The immunoreactivities of humans were absolutely corresponding to that of this vervet monkey. According to these facts, we assumed that these antibodies recognized suitable TTR and Aβ amyloid lesions in vervet monkeys, as well as humans. On the other hand, as for IAPP, detail immunohistochemical information of an antibody to IAPP 7–17 residue used in this study has not been described, while similar antibodies to IAPP 8–17 residue reacted well with intact islet amyloid in humans and cats.[6] The immunoreactivity of an antibody to IAPP 8–17 was consistent with that of an antibody to IAPP 7–17. Those IAPP residues are conserved between various mammalian species, and IAPP 8–20 is known as the second major constituent of islet amyloid.[5] Therefore, we assumed that the antibody to IAPP used in this study reacted precisely with intact islet amyloid of this monkey species.

SSA is one of the common systemic amyloidoses in humans, occurring in 25% of people who are older than 80 years.[15] SSA has been previously called cardiac amyloidosis because it shows cardiac symptoms, such as heart failure and/or arrhythmia, due to severe amyloid deposition in the heart.[15] As for histopathologic characteristics of SSA in humans, the organ most severely affected by amyloid deposition is the heart, while deposition is also found in the other systemic organs. On the other hand, there are few amyloid deposits in the liver, spleen, and kidney, except the renal pelvis, which are frequent organs for other types of systemic amyloidoses, such as AA or AL amyloidosis.[15] These histopathologic features in humans are consistent with those in the vervet monkey. Furthermore, clinical symptoms, such as arrhythmia, and biochemical aspects of the amyloid precursor, such as TTR and not AA or AL, in humans, correspond to the characteristics in the vervet monkey.[14] Another manifestation of TTR amyloid deposition is familial or hereditary TTR amyloidosis, which is known as familial amyloid polyneuropathy (FAP).[15] FAP patients with a variant TTR reveal onset of cardiac symptoms and severe systemic TTR amyloidosis usually the third decade of life, with deposits especially prominent in the heart and peripheral nervous system.[13] Because there is no information for TTR amino acid sequence and its mutant in vervet monkeys, the hereditary aspect of TTR amyloidosis could not be considered in the present study. However, the clinical, histologic, and immunohistochemical features suggest that the monkey suffered from SSA and not FAP, because the monkey was very old (a 29-year-old monkey corresponds nearly to an 85-year-old human) and because amyloid was deposited exclusively in the heart rather than in the peripheral nerves.

Teng and colleagues[14] reported that transgenic mice overexpressing human wild-type *TTR* gene revealed predominant deposits of TTR-positive and DFS-negative materials in the heart and kidney. This type of deposit is consistent with the deposits in the testes of the vervet monkey in this study. Namely, the deposits in TTR transgenic mice and this vervet monkey may be considered immature materials before amyloid fibril formation.[14]

Cerebral amyloidosis consisting of Aβ is an aging-related amyloidosis, although it occurs earlier and is significantly developed in Alzheimer's disease.[6,8] SPs and CAA as histopathologic hallmarks in Alzheimer's disease also appear in aged nonhuman primates.[7] SPs in cynomolgus monkeys are morphologically classified into neuritic and diffuse plaques; the neuritic plaques are more frequently observed than the diffuse ones, whereas CAA is more frequently found in capillaries than in meningeal arterioles.[7] Findings of abundant neuritic plaques and predominant capillary CAA rather than meningeal CAA have been described previously, in the first study of SPs and CAA in a vervet monkey.[4] The characteristics of SPs and CAA in the present study are consistent with the previous studies of cynomolgus monkeys.[7]

Islet amyloidosis consisting of IAPP often appears as one of the aging-related changes in aged primates including humans,[3] while this amyloid deposition is accelerated in diabetes mellitus.[13] Because the vervet monkey did not have any history for diabetes, possibilities are considered that the islet amyloid deposition in this monkey likely occurred as an aging-related change and that degrading insulin secretion in the absence of fasting hyperglycemia was associated with an increase of IAPP aggregation and the onset of islet amyloidosis.[3] This type of amyloid deposition has been previously reported in various primate species, that is, humans and macaque monkeys.[10,13] Morphologic and immunohistochemical characteristics of islet amyloidosis in vervet monkey are consistent with those in other primate species.[10]

ApoE and AP are often colocalized with various types of amyloid precursors, such as Aβ, prion protein, AA, and IAPP[7,9,13] and accelerate in vitro fibril formation of the amyloids.[1] Although in vitro data on the correlation between apoE and TTR have not been confirmed previously, the colocalization of apoE in the TTR amyloid portion suggests that TTR amyloid deposition might be accelerated by apoE and AP, as well as other types of amyloids.[13] In summery, 3 different aging-related amyloidoses were found in an

aged vervet monkey. TTR amyloidosis has only been reported in SAMP mice,[2] while this is the first spontaneous case report on TTR amyloidosis in mammalian species, other than humans and experimental animals with a special genetic background.

Acknowledgement

The authors thank Ms. Chieko Ohno for her technical help.

References

1 Hass S, Fresser F, Kochl S, Beyreuther K, Utermann G, Baier G: Physical interaction of ApoE with amyloid precursor protein independent of the amyloid Aβ region in vitro. J Biol Chem **273:**13892–13897, 1998

2 Higuchi K, Naiki H, Kitagawa K, Hosokawa M, Takeda T: Mouse senile amyloidosis: ASSAM amyloidosis in mice presents universally as a systemic age-associated amyloidosis. Virchows Arch B Cell Pathol Incl Mol Pathol **60:**231–238, 1991

3 Hull RL, Westermark GT, Westermark P, Kahn SE: Islet amyloid: a critical entity in the pathogenesis of type 2 diabetes. J Clin Endocrinol Metab **89:**3629–3643, 2004

4 Lemere CA, Beierschmitt A, Iglesias M, Spooner ET, Bloom JK, Leverone JF, Zheng JB, Seabrook TJ, Louard D, Li D, Selkoe DJ, Palmour RM, Ervin FR: Alzheimer's disease Aβ vaccine reduces central nervous system Aβ levels in a non-human primate, the Caribbean vervet. Am J Pathol **165:**283–297, 2004

5 Mazor Y, Gilead S, Benhar I, Gazit E: Identification and characterization of a novel molecular-recognition and self-assembly domain within the islet amyloid polypeptide. J Mol Biol **322:**1013–1024, 2002

6 Ma Z, Westermark GT, Johnson KH, O'Brien TD, Westermark P: Quantitative immunohistochemical analysis of islet amyloid polypeptide (IAPP) in normal, impaired glucose tolerant, and diabetic cats. Amyloid **5:**255–256, 1998

7 Nakamura S, Kiatipattanasakul W, Nakayama H, Ono F, Sakakibara I, Yoshikawa Y, Goto N, Doi K: Immunohistochemical characteristics of the constituents of senile plaques and amyloid angiopathy in aged cynomolgus monkeys. J Med Primatol **25:**294–300, 1996

8 Nagele RG, D'Andrea MR, Anderson WJ, Wang HY: Intracellular accumulation of β-amyloid$_{1-42}$ in neurons is facilitated by the alpha 7 nicotinic acetylcholine receptor in Alzheimer's disease. Neuroscience **110:**199–211, 2002

9 Namba Y, Tomonaga M, Kawasaki H, Otomo E, Ikeda K: Apolipoprotein E immunoreactivity in cerebral amyloid deposits and neurofibrillary tangles in Alzheimer's disease and kuru plaque amyloid in Creutzfeldt-Jakob disease. Brain Res **541:**163–166, 1991

10 O'Brien TD, Wagner JD, Litwak KN, Carlson CS, Cefalu WT, Jordan K, Johnson KH, Butler PC: Islet amyloid and islet amyloid polypeptide in cynomolgus macaques (*Macaca fascicularis*): an animal model of human non-insulin-dependent diabetes mellitus. Vet Pathol **33:**479–485, 1996

11 Podlisny MB, Tolan DR, Selkoe DJ: Homology of the amyloid β protein precursor in monkey and human supports a primate model for β amyloidosis in Alzheimer's disease. Am J Pathol **138:**1423–1435, 1991

12 Sawabe M, Hamamatsu A, Ito T, Arai T, Ishikawa K, Chida K, Izumiyama N, Honma N, Takubo K, Nakazato M: Early pathogenesis of cardiac amyloid deposition in senile systemic amyloidosis: close relationship between amyloid deposits and the basement membranes of myocardial cells. Virchows Arch **442:**252–257, 2003

13 Sipe JP: 2005 Amyloid Proteins, 1st ed., pp. 3–27, pp. 180–181, pp. 385–406, pp. 732–742. WILEY-VCH, Weinheim, Germany, 2005

14 Teng MH, Yin JY, Vidal R, Ghiso J, Kumar A, Rabenou R, Shah A, Jacobson DR, Tagoe C, Gallo G, Buxbaum J: Amyloid and nonfibrillar deposits in mice transgenic for wild-type human transthyretin: a possible model for senile systemic amyloidosis. Lab Invest **81:**385–396, 2001

15 Westermark P, Bergstrom J, Solomon A, Murphy C, Sletten K: Transthyretin-derived senile systemic amyloidosis: clinicopathologic and structural considerations. Amyloid **10**(Suppl 1)**:** 48–54, 2003

Request reprints from Shinichiro Nakamura, Research Center for Animal Medical Science, Shiga University of Medical Science, Seta-Tsukinowa-Cho, Ohtsu, Shiga 520-2192 (Japan). E-mail: snakamur@belle.shiga-med.ac.jp.

Exp. Anim. 57(4), 385–395, 2008

Type 2 Diabetes Mellitus in a Non-Obese Mouse Model Induced by Meg1/Grb10 *Overexpression*

Yoshie YAMAMOTO[1,2], Fumitoshi ISHINO[3], Tomoko KANEKO-ISHINO[4], Hirosuke SHIURA[3], Kozue UCHIO-YAMADA[5], Junichiro MATSUDA[5], Osamu SUZUKI[5], and Katsunori SATO[2]

[1]Department of Veterinary Science, National Institute of Infectious Diseases, 1–23–1 Toyama, Shinjuku-ku, Tokyo 162-8640, [2]Okayama University Graduate School of Natural Science and Technology, 3–1–1 Tsushima-naka, Okayamashi, Okayama 700-8530, [3]Department of Epigenetics, Medical Research Institute, Tokyo Medical and Dental University, 1–5–45 Yushima, Bunkyou-ku, Tokyo 113-8510, [4]Tokai University School of Health Sciences, Bohseidai, Isehara, Kanagawa 259-1193, and [5]Division of Biomedical Research Resources, National Institute of Biomedical Innovation, 7–6–8 Saito-Asagi, Ibaraki, Osaka 567-0085, Japan

Abstract: *We assessed the possibility of C57BL/6-Tg (*Meg1/Grb10*)isn(Meg1 Tg) mice as a non-obese type 2 diabetes (2DM) animal model. Meg1 Tg mice were born normal, but their weight did not increase as much as normal after weaning and showed about 85% of normal size at 20 weeks of age. Body mass index of Meg1 Tg mice was also smaller than that of control mice. The glucose tolerance test and insulin tolerance test showed that Meg1 Tg mice had reduced ability to normalize the blood glucose level. Blood urea nitrogen (BUN) in Meg1 Tg mice (19.6 ± 1.2 mg/dl) was significantly lower than in controls (22.0 ± 0.8 mg/dl), while plasma triglyceride, insulin, adiponectin, and resistin levels were significantly higher (202.0 ± 23.4 mg/dl vs 146.3 ± 23.4 mg/dl, 152.4 ± 16.3 pg/ml vs 88.1 ± 16.9 pg/ml, 74.4 ± 10.9 μg/ml vs 48.3 ± 7.0 μg/ml, and 4.0 ± 0.2 ng/ml vs 3.6 ± 0.2 ng/ml, respectively). Body, visceral fat weight and liver weights were significantly lower (19.6 ± 0.4 g vs 24.3 ± 0.3 g, 376.7 ± 29.6 mg to 507.5 ± 23.0 mg, and 906.0 ± 41.8 mg to 1,001.0 ± 15.1 mg, respectively). Thus, hyperinsulinemia observed in Meg1 Tg mice indicates that their insulin signaling pathway is somehow inhibited. With high fat diet, the diabetes onset rate of Meg1 Tg mice increased up to 60%. These results suggest that Meg1 Tg mice resemble human 2DM.*

Key words: *biochemical characterization,* Meg1/Grb10 *transgenic mouse, non-obese mouse model, type 2 diabetes mellitus*

Introduction

Type 2 diabetes mellitus (2DM) is a life-threatening endocrine disorder that affects as many as 6% to 10% of the population of the world. This type of diabetes is classified as non-insulin dependent diabetes and accounts for higher than 95% of all cases of diabetes [12, 39]. Moreover, recent studies have revealed that the prevalence of 2DM has doubled in the United States over the last 30 years [1].

(Received 2 November 2007 / Accepted 24 March 2008)

Address corresponding: Y. Yamamoto, Department of Veterinary Science, National Institute of Infectious Diseases, 1–23–1 Toyama, Shinjuku-ku, Tokyo 162-8640, Japan

Many experimental 2DM model animals have been established from spontaneous mutants and are currently in use in human 2DM research [11, 22, 24, 33, 35]. In spite of much effort, which has focused on using such model animals, some aspects of 2DM remain unclear. To elucidate the pathological character of 2DM, it is necessary to identify which metabolic pathways are responsible for the onset of 2DM. However, in many cases, the relationship between original mutations and their affected metabolic pathways is difficult to explain. Recent progress in molecular biology has enabled us to take another approach to develop novel diabetes model animals through the manipulation of genes that are closely related to glucose metabolism and insulin resistance [6]. Using gene-targeting technology, a number of useful mouse models have recently been developed for the study of the progression of diabetes [4, 17].

Recently, genomic imprinting has been discovered as an important factor in the etiology of 2DM. A number of studies have reported a relationship between genomic imprinting and 2DM in the mouse [13, 21, 30]. Overexpression of some imprinted genes might explain the mechanism of human transient neonatal diabetes [21], and deletion of some imprinted genes has been suggested as the cause of pancreatic β cell dysfunction [13]. Another candidate imprinted gene for 2DM is maternally expressed 1(Meg1)/ growth factor receptor-binding protein (Grb) 10 [23]. Recently, it has been reported that *Meg1/Grb10* knockout mice show the embryonic overgrowth phenotype [3]. *Meg/Grb10* transgenic mice Meg1 Tg mice were produced to elucidate Meg1/Grb10 function *in vivo* [31]. Grb10 interacts with both insulin receptors (IR) and insulin-like growth factor I receptors (IGF-1R) *in vitro* [8, 9, 27]. Since the IGF-1 signaling pathway is reportedly involved in embryonic growth, Meg1/Grb10 may have a negative effect both on the embryonic growth and postnatal growth phenotypes associated with uniparental duplication of chromosome 11 [7, 23]. Alternatively, Meg1/Grb10 may function in glucose homeostasis, which is regulated by the IR signaling pathway. Insulin binds to IR and activates a signal transduction pathway through its receptor kinase activity. It has been demonstrated that IGF1 functions via IGF1R, while IGF2 functions via both IGF1R and IR, and that each of these signaling pathways contributes to some extent to late embryonic growth [20]. Moreover, mutation studies of human 2DM patients indicate the existence of additional factors in the pathogenesis of this disease [25].

Overall, Meg1 Tg mice have similar character to human 2DM in overexpression of the imprinted Meg1/Grb10 gene that functions negatively for both insulin signaling via IR and IGF-1 signaling via IGF-1R. Therefore, it seems likely that, in the late embryonic stage, when endogenous Meg1/Grb10 expression is very high, Meg1/Grb10 negatively regulates growth via modulation of both the IR and IGF1R cascades [31]. There are few data about biochemical changes in the Meg1 Tg mouse. To be useful in therapeutic research the model mouse has to show a similar phenotype to human 2DM. Furthermore, the incidence rate of the onset of 2DM in Meg1 Tg mice fed on basal diet was reportedly small [30].

In this study, we examined several basic biochemical characters of Meg1 Tg mice as a 2DM model, and the effects of diet on the onset of 2DM. The results indicate that the Meg1 Tg mouse is a useful non-obese 2DM mouse model.

Materials and Methods

Animals

The production and maintenance of *Meg1/Grb10* transgenic mice were reported in detail at elsewhere [31]. Transgenic (C57BL X C3H) F_2 mice were screened by PCR amplification of tail DNA samples using transgene-specific and endogenous Peg1 primer sets. Transgenic-positive founder mice (Meg1 Tg mouse) were backcrossed to C57BL/6NJcl (C57BL/6) mice, and the litters that were used in subsequent studies contained animals that were maintained within the C57BL/6 hybrid background. The Meg1 Tg mouse consists of 4 lines, with names of T10L, T18L, T20L, and T27L. We used these 4 lines for each experiment. Transgenic-negative mice were used as control mice. C57BL/6, NOD/ShiJcl (NOD), KK-A^y/TaJcl (KK-A^y), and BKS.Cg-*+Lepr^{db}*/*+Lepr^{db}*/Jcl (BKS) mice were also used in the RT-PCR experiment. Only male mice were used in our experiment.

This study was performed in accordance with the *Guidelines for Animal Experimentation of the National*

Institute of Infectious Diseases.

Body weight and body mass index (BMI)

Body weights of all mice used in our experiments were measured weekly from 4 weeks of age to 20 weeks. At 15 weeks of age, mouse length from nose to anus was recorded. Body mass index (BMI) was calculated as body weight (g) / body length^2 (cm).

Food and water intake

The mice were allowed free access to food pellets and water. We used either CMF (Oriental yeast Co., Ltd., Tokyo) or Quick Fat (CLEA Japan, Inc., Tokyo) for normal fat diet (NFD) and high fat diet (HFD), respectively. HFD contains high crude fat and glucose, which gives it a higher calorie count than NFD. Food intake per mouse was calculated as the average of 3 days intake at 11 weeks of age.

Organ weight

At 30 weeks of age 5 Meg1 Tg mice and control mice were sacrificed under deep ether anesthesia and necropsied. Visceral fat and livers were separated and weighed.

Glucose tolerance test and insulin tolerance test

Glucose tolerance tests and insulin tolerance test were performed on 11-week-old Meg1 Tg mice that had been fed on HFD. Glucose tolerance tests and insulin tolerance tests were performed after overnight fasting by administering glucose orally (2.0 g/kg body weight) and 0.3 μl of blood was collected from the tail vain after 0, 30, 60, and 120 min. The blood glucose level was measured by FreeStyle Meter (NIPRO, Osaka). Insulin tolerance tests were performed by an intraperitoneal injection of 1.0 U/kg of human insulin (Eli Lilly Japan, Tokyo) to Meg1 Tg mice and control mice; then 0.3 μl of blood was collected from the tail vein after 0, 30, 60, and 90 min. The blood glucose level was measured by FreeStyle Meter (NIPRO).

Plasma chemistry

Meg1 Tg and control mice were maintained on a normal light/dark cycle. Blood was collected from the mice with heparin at necropsy and inspection. The samples were centrifuged at 13,000 rpm centrifugation, and plasma was collected and stored at –30°C until assay. Plasma leptin, adiponectin, insulin and resistin were assayed by ELISA. Plasma total glucose, total cholesterol (TCHO), ammonia, triglyceride (TG), blood urea nitrogen (BUN), GOT, GPT, ALP, CPK, and LDH were measured using Fuji dry-chem 3000 (FUJIFILM Medical Co., Ltd., Tokyo). Livers and visceral adipose tissues were also recorded.

Histology

For histopathology, pancreas tissue samples were taken from Meg1 Tg and control mice at 20 weeks of age. The tissue samples were fixed in 10% buffer-neutralized formalin solution and embedded in paraffin. Sections were cut at 2 μm thickness and stained with hematoxylin and eosin.

Urinalysis and confirmation of the onset of 2DM

Urine collection was executed by compulsive urination at each weighing time, and urinary glucose was determined by Urolabostick (Biel-Sankyo Co., Ltd., Tokyo). When urinary glucose was detected, blood was collected from the tail vein. Confirmation of the onset of 2DM was decided by the detection of over 300 mg/ml of glucose in blood.

RT-PCR

Total RNA was extracted from livers, pancreata, skeletal muscles, and white and brown adipose tissues from 5 mice each of the Meg1 Tg, NOD, KK-A^y, BKS, and C57BL/6 strains of mice at 11 weeks of age, using the RNeasy system (QIAGEN K. K., Tokyo) according to the manufacturer's instructions. For the RT-PCR analysis, cDNA was synthesized from 1 μg of the total RNA using the SuperScript III First-Strand cDNA Synthesis System (Invitrogen Japan K. K., Tokyo) according to the manufacturer's instructions. The cDNA was PCR-amplified in 50 μl of reaction mixture containing 25 μl of TaqMan master mix (Applied Biosystems Japan Ltd., Tokyo) and 500 nM of the gene-specific (*Meg1/Grb10*, uncoupling protein 1 (*Ucp1*), glucose transporter 4 (*Glut4*), and *G3PDH* for normalization) TaqManProbe. The assays were performed in triplicate and the copy number of the *Meg1/Grb10*, *Ucp1*, and *Glut4* RNA were

calculated with an ABI Prism 7900 Sequence Detector (Applied Biosystems Japan). The data for each tissue were normalized to an internal standard (*G3PDH*).

Statistical analysis

Measurement data are shown as the mean value ± standard error (Mean ± SE). Statistical analysis of the data was performed using a one-factor ANOVA followed by Student's *t*-test. Comparison of the mean was calculated by Bonferroni's method. Covariance analysis was performed by Levene's method. Calculation of confidence limits and significance testing were made at a level of P=0.05.

Results

Postnatal growth curve

Fig. 1 shows the body weights of Meg1 Tg mice and controls that were fed either normal fat diet (NFD) or high fat diet (HFD). The weight of Meg1 Tg mice was normal until 4 weeks of age under both NFD and HFD diet conditions. However, their body weights did not increase as much as control mice after weaning and were 12 to 15% smaller than these of control mice at 20 weeks of age. These differences were statistically significant (P<0.05).

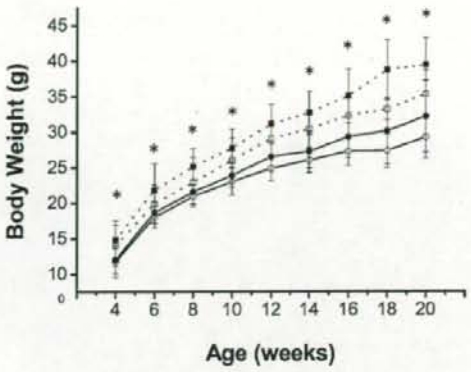

Fig. 1. Growth curve of control and Meg1 Tg mice from 4 to 20 weeks of age. Plotted values are means ± SE for 20 mice per group. Open square (□), control mice fed NFD; filled square (■), control mice fed HFD; open circle (○), Meg1 Tg mice fed NFD; filled circle (●), Meg1 Tg mice fed HFD. *P<0.05 (Student's *t*-test).

Food intake and BMI

For average food intake, no differences were observed between Meg1 Tg mice and controls under both diet conditions at 11 weeks of age (Fig. 2A: fed with HFD, 1.74 ± 0.02 g/day/10 g of body weight vs 1.65 ± 0.03 g/day/10 g of body weight; and with NFD, 1.65 ± 0.02 g/day/10 g of body weight vs 1.51 ± 0.07 g/day/10 g of body weight). However, BMI of Meg1 Tg mice were significantly lower than these of control mouse fed with HFD (P<0.05) both at 15 and 30 weeks of age (Fig. 2B: BMI at 15 weeks of age, 0.27 ± 0.01 g/cm^2 vs 0.32 ± 0.03 g/cm^2; and at 30 weeks of age, 0.29 ± 0.05 g/cm^2 vs 0.36 ± 0.07 g/cm^2).

Glucose tolerance test and insulin tolerance test

The plasma glucose level of Meg1 Tg mice fed with HFD at 11 weeks of age was significantly higher than those in both Meg1 Tg mice and controls fed with NFD (P<0.05), indicating that their glucose tolerance was reduced (Fig. 3A). The reduction in blood glucose concentration after intraperitoneal administration of insulin was significantly delayed in Meg1 Tg mice compared to control mice fed with either HFD or NFD (P<0.05), indicating that Meg1 Tg mice had insulin resistance (Fig. 3B).

Organ weight

The weights of body, visceral fat, and liver, and the visceral fat/body weight ratios and liver/body weight ratios of Meg1 Tg and control mice at 10 to 12 weeks of age are shown in Table 1. The effect on organ weight by HFD feeding in Meg1 Tg mice was examined. When mice were fed HFD, weights of body, visceral fat and livers of Meg1 Tg mice were significantly lower than the controls (P<0.05), while liver/body weight ratio of Meg1 Tg mice was significantly higher than that of control mice (P<0.05). When Meg1 Tg mice were fed NFD, their body weight was significantly lower than the controls (P<0.05). There were no differences in visceral fat/body weight and liver/body weight ratios between Meg1 Tg and control mice irrespective of diet.

Plasma chemistry

The data on BUN, TG, insulin, adiponectin, resistin,

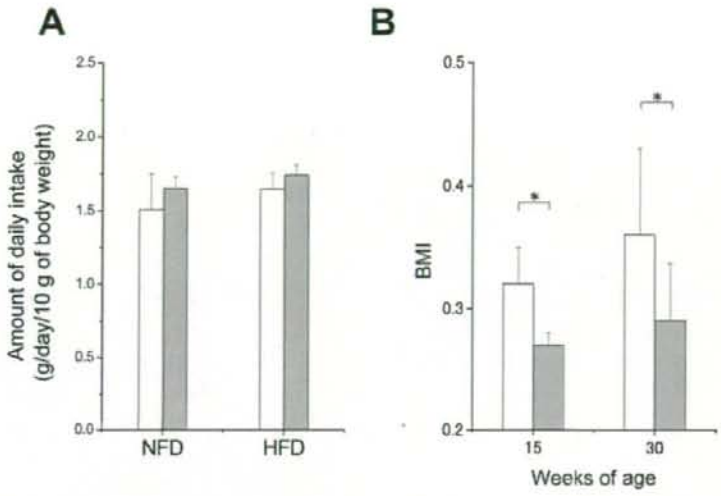

Fig. 2. Daily intake and BMI change in control and Meg1 Tg mice. (A) Daily intake of Meg1 Tg (▩) and control (□) mice at 11 weeks of age that were fed with NFD or HFD. There were no significant differences between the diet groups. (B) BMI of Meg1 Tg and control mice fed with HFD were calculated at 15 and 30 weeks of age. BMI of Meg1 Tg mice (▩) at both ages were significantly lower than those of control mice (□) ($P<0.05$).

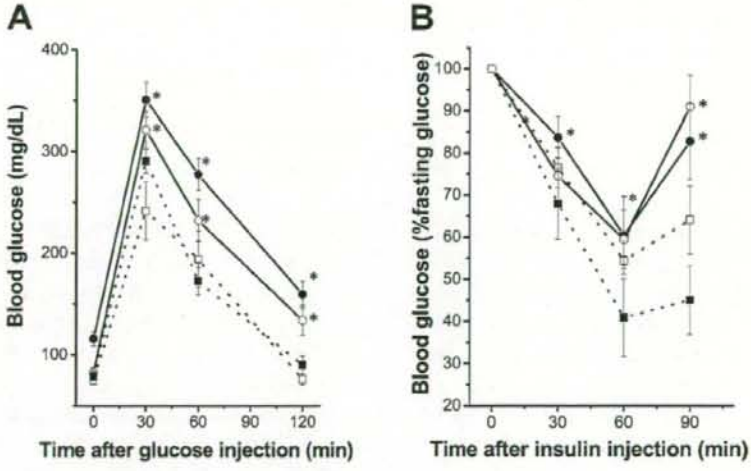

Fig. 3. Glucose and insulin tolerance level of Meg1 Tg and control mice. (A) Glucose tolerance in mice at 11 weeks of age that had been fasted overnight (n=10). (B) Insulin tolerance in mice at 11 weeks of age that had been fasted overnight (n=10). Plotted values are means ± SE for 10 mice per group. Open square (□), control mice fed NFD; filled square (■), control mice fed HFD; open circle (○), Meg1 Tg mice fed NFD; filled circle (●), Meg1 Tg mice fed HFD. *$P<0.05$ (Student's *t*-test). Glucose levels and their reduction rate in Meg1 Tg mice were significantly higher than in control mice.

Table 1. Liver, fat, and body weights of Meg1Tg and control mice at 10 to 12 weeks of age

	Control (NFD)	Meg1 Tg (NFD)	Control (HFD)	Meg1 Tg (HFD)
Body weight (g)	20.8 ± 0.6	18.4 ± 0.3[a)]	24.3 ± 0.3	19.6 ± 0.4[a)]
Visceral fat weight (mg)	197.6 ± 46.0	187.0 ± 68.6	507.5 ± 23.0	376.7 ± 29.6[a),b)]
Visceral fat/body weight ratio (mg/g)	9.0 ± 0.9	8.9 ± 1.6	18.8 ± 2.6	20.0 ± 1.1
Liver weight (mg)	900.2 ± 30	977.4 ± 38.5	1,001.0 ± 15.1	906.0 ± 41.8[a)]
Liver/body weight ratio (mg/g)	44.5 ± 3.7	51.6 ± 4.9	41.2 ± 1.3	44.9 ± 2.1[a)]

Values are the means ± SE for 10 mice per control and 10 mice per Meg1Tg. Meg1Tg (HFD) and control (HFD) mice were fed HFD. Meg1Tg (NFD) and control (NFD) mice were fed NFD. [a)]$P<0.05$ vs control, [b)]$P<0.05$ vs Meg1 Tg (NFD).

Table 2. Plasma chemistry in Meg1 Tg and control mice at 10 to 12 weeks of age

	Control (NFD)	Meg1 Tg (NFD)	Control (HFD)	Meg1 Tg (HFD)
BUN (mg/dl)	26.7 ± 1.9	20.6 ± 0.7	22.0 ± 0.8	19.3 ± 1.2[a)]
Triglyceride (mg/dl)	69.3 ± 23.2	90.6 ± 21.9	146.3 ± 11.4	202.0 ± 23.4[a),b)]
Insulin (pg/ml)	92.5 ± 13.4	153.3 ± 14.3	88.1 ± 16.9	152.4 ± 16.3[a)]
Adiponectin (ng/ml)	23 ± 4.01	46.8 ± 3.2	48.3 ± 7.0	74.4 ± 10.9[a),b)]
Resisitin (ng/ml)	2.28 ± 0.2	3.3 ± 0.2	3.6 ± 0.2	4.0 ± 0.2
IGF-1 (ng/ml)	395.8 ± 43.1	232.5 ± 28.3	358 ± 49.5	272.1 ± 24.4
Leptin (pg/ml)	548 ± 171	1,136.0 ± 267.0	1,036.0 ± 161.0	1,008.0 ± 146.0
NH3 (μg/dl)	143.1 ± 24.2	162.0 ± 12.2	223.1 ± 32.6	280.7 ± 50.9[b)]
Glucose (mg/dl)	161 ± 16.9	163.0 ± 12.6	172.8 ± 9.4	199.7 ± 58.4

Values are the means ± SE for 10 mice per control and 10 mice per Meg1Tg. Meg1Tg (HFD) and control (HFD) mice were fed bHFD. Meg1Tg (NFD) and control (NFD) mice were fed NFD. [a)]$P<0.05$ vs control, [b)]$P<0.05$ vs Meg1Tg(NFD).

IGF-1, leptin, ammonium, and glucose, measured at 10 to 12 weeks of age, are shown in Table 2. Irrespective of diet, plasma BUN in Meg1 Tg mice was significantly lower than in control mice ($P<0.05$). Plasma TG, insulin adiponectin and resistin in Meg1 Tg mice were significantly higher than in control mice ($P<0.05$), whereas plasma IGF-1 of Meg1 Tg mice tended to be lower than in controls. When mice were fed NFD, the plasma leptin concentration of Meg1 Tg mice was significantly higher than that of control mice. For, mice fed HFD, the plasma leptin level of Meg1 Tg mice was almost the same as the value of control mice (Table 2). Plasma glucose and ammonia in both NFD- and HFD-fed Meg1 Tg mice tended to be higher than those of control mice.

Other measured biochemical markers such as TCHO, GOT, GPT, ALP, CPK, and LDH plasma concentrations measured in Meg1 Tg and control mice of the same age were almost similar (data not shown).

Histological analysis

We found two histological abnormalities in the pancreatic tissues of Meg1 Tg mice fed NFD: atrophy of the pancreatic acinus cells and an increase in adipocytes at 20 weeks of age; and enlargement of islet of Langerhans (Fig. 4B). When Meg1 Tg mice were fed HFD, the above-noted pathological abnormalities were more severe than these of NFD feeding (Fig. 4C). Pathological abnormalities did not develop in control mice fed NFD or HFD (Fig. 4A).

The onset rate of type 2 diabetes

The onset rates of 2DM between Meg1 Tg mouse fed NFD and HFD at 25 weeks were 11.3% and 60.0%, respectively (Fig. 5A). This clearly demonstrates that feeding with HFD induces 2DM in Meg1 Tg mice. There were no symptoms of 2DM in control mice up to 30 weeks of age.

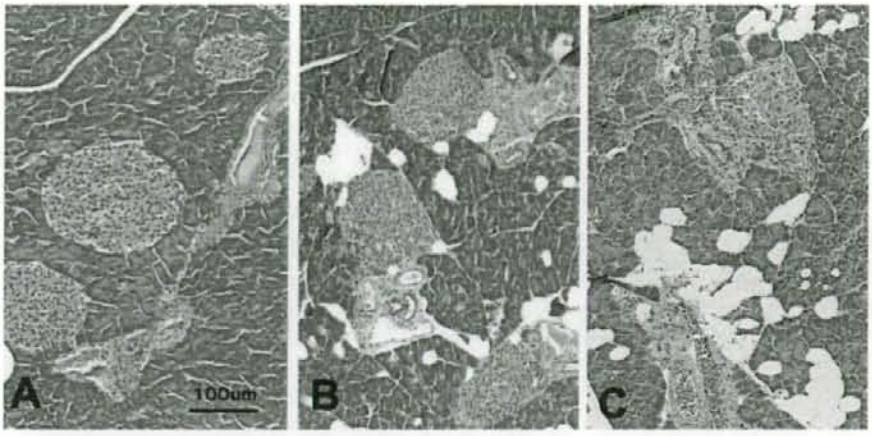

Fig. 4. Light microscopic features of pancreata from control and Meg1 Tg mice around 20 weeks of age. Heamatoxylin and eosin stain, × 100. (A) Control mouse. (B) Meg1 Tg mouse fed NFD. (C) Meg1 Tg mouse fed HFD. Vacuolation and denaturation at exocrine pancreas in the Meg1 Tg mouse was found. Furthermore, enlargement of an islet of Langerhans was observed. The pathological abnormality of Meg1 Tg mice fed HFD was more severe than that of NFD-fed Meg1 Tg mice.

Meg1/Grb10, Ucp1, *and* Glut4 *expression in Meg1 Tg and 3 diabetes model mice*

For further analytical research, we examined diabetes related gene expressions of Meg1 Tg mice in comparison with NOD, KK-A^y, BKS, and C57BL/6 mice. *Meg1/Grb10*, *Ucp1*, and *Glut4* expression ratios against control gene are shown in Fig. 6. *Meg1/Grb10* gene expression of skeletal muscle of Meg1 Tg mice was 100 times higher than those of the other 3 diabetes model mice and the C57BL/6 mouse (Fig. 6A: $P<0.05$). In contrast, *Glut4* expression of skeletal muscle of Meg1 Tg mice was significantly lower than these of the 3 diabetes model mice and the C57BL/6 mouse (Fig. 6C: $P<0.05$). There were no differences of *Ucp1* gene expression in brown adipose tissue between Meg1 Tg and the 3 diabetes model mice and the C57BL/6 mouse. Meg1 Tg mice fed HFD showed suppression of *Ucp1* gene expression in brown adipose tissue (Fig. 6).

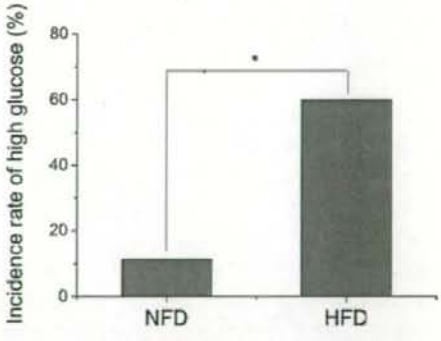

Fig. 5. Increased incidence rate of high blood glucose in Meg1 Tg mice fed HDF. Meg1 Tg mice were fed NFD and HFD for 25 weeks. The onset rates (■) of type 2 diabetes, the decided by the detection of over 300 mg/ml of glucose in the blood, in the Meg1 Tg mouse were compared by diet. HFD feeding-induced diabetes was significantly higher than NFD feeding. *$P<0.05$ (Student's t-test).

Discussion

We evaluated the Meg1 Tg mouse as a non-obese 2DM animal model in this study. Two of the major defects seen in 2DM are insulin resistance of targets, such as liver, muscle and adipose tissues, and impaired insulin secretion from pancreatic β-cells [26, 37, 38]. Histological analysis revealed the pancreatic abnormality in Meg1 Tg mice (Fig. 4). Moreover, Meg1 Tg mice showed both the insulin resistance and glucose intoler-

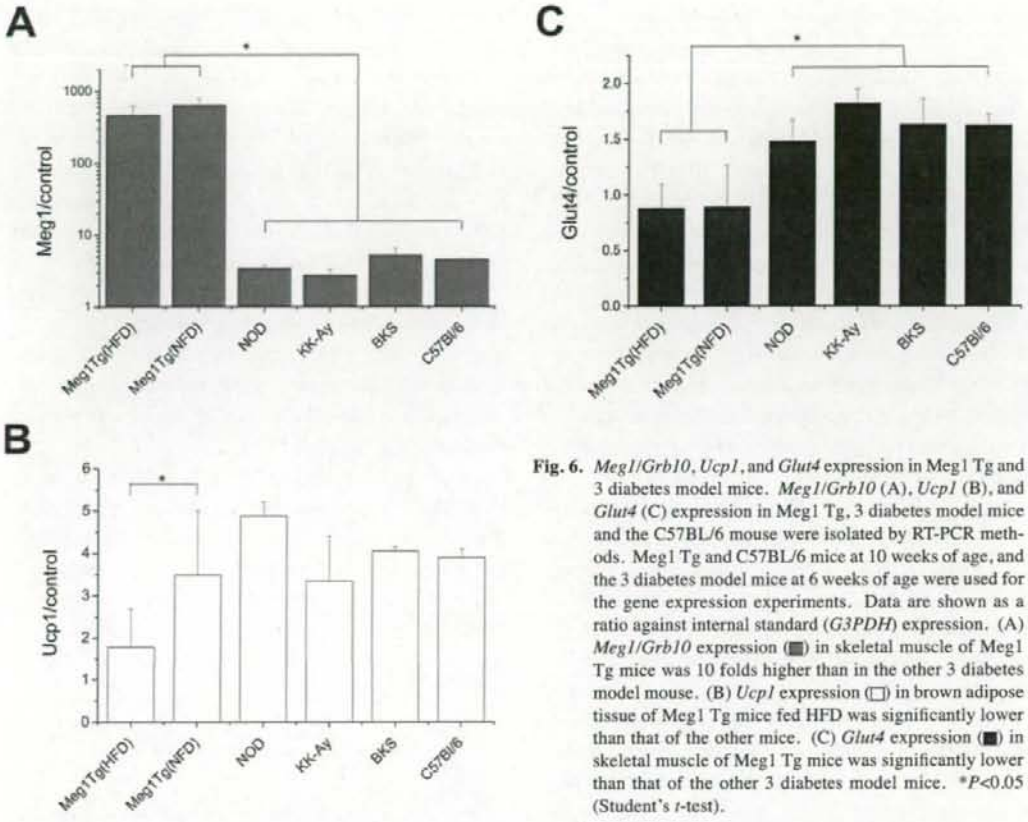

Fig. 6. *Meg1/Grb10*, *Ucp1*, and *Glut4* expression in Meg1 Tg and 3 diabetes model mice. *Meg1/Grb10* (A), *Ucp1* (B), and *Glut4* (C) expression in Meg1 Tg, 3 diabetes model mice and the C57BL/6 mouse were isolated by RT-PCR methods. Meg1 Tg and C57BL/6 mice at 10 weeks of age, and the 3 diabetes model mice at 6 weeks of age were used for the gene expression experiments. Data are shown as a ratio against internal standard (*G3PDH*) expression. (A) *Meg1/Grb10* expression (■) in skeletal muscle of Meg1 Tg mice was 10 folds higher than in the other 3 diabetes model mouse. (B) *Ucp1* expression (□) in brown adipose tissue of Meg1 Tg mice fed HFD was significantly lower than that of the other mice. (C) *Glut4* expression (■) in skeletal muscle of Meg1 Tg mice was significantly lower than that of the other 3 diabetes model mice. $*P<0.05$ (Student's *t*-test).

ance (Fig. 3). The plasma insulin concentration of Meg1 Tg mice was significantly higher than in control mouse (Table 2). These data demonstrate that the dysregulation of plasma glucose was caused by insulin resistance. Our results provide support for Meg1 Tg mouse as a 2DM mouse model. Moreover, the body weights of Meg1 Tg neonates were slightly lower than controls, and this difference increased with growth up to 12 to 15% of body weight. BMI of Meg1 Tg mice was also smaller than control mice (Figs. 1 and 2). Body, visceral fat weight and liver weights were also slightly lower in Meg1 Tg mice than in control mice. However, the visceral fat/body weight and liver/body weight ratios of Meg1 Tg mice were similar to those of control mice (Table 1). Overall, the Meg1 Tg mouse showed a non-obese mouse character.

There are several spontaneous polygenic models of 2DM, such as the OLETF rat, the KK-A^y mouse, the NSY mouse, and the BKS mouse, which develop overt obesity and hyperinsulinemia prior to the onset of diabetes [7, 14, 34]. The KK-A^y mouse and the BKS mouse showed obesity compared with controls [33, 35]. However, the Meg1 Tg mouse model showed a non-obese character. Only limited data exist for 2DM in Japanese subjects, probably because Japanese people are relatively lean. Some Japanese 2DM patients are non-obese patients and the causal factors of 2DM onset is being analyze by many laboratories [15, 28]. The Meg1 Tg diabetes mouse model may provide a useful tool for these researches.

Biochemical analysis data of the Meg1 Tg mouse demonstrated metabolic abnormality. Plasma BUN in

Meg1 Tg mice was significantly lower than in control mice. Plasma TG, insulin, adiponectin, and resistin levels of HFD-fed Meg1 Tg mice were significantly higher than those of control mice. The mean concentration of TG in Meg1 Tg mice, especially with HFD feeding, was over 200 mg/dl, a condition that is called high-fat plasma. High-fat plasma is said to be a precursor of diabetes [19]. A high level of plasma adiponectin and low BMI were found in Meg1 Tg mice fed HFD (Fig. 2B). There was an inverse correlation between plasma adiponectin and BMI in the Meg1 Tg mouse (data not shown). This shows that the Meg1 Tg mouse has characteristics similar to human 2DM. The circulating IGF-1 level in Meg1 Tg mice tended to be lower than that of control mice (Table 2). A lower IGF-1 level could explain the lower body weight of the Meg1 Tg mouse due to the role of IGF-1 signaling in postnatal growth [10]. Overall, the biochemical data suggest that HFD feeding in the Meg1 Tg mouse induces human 2DM related characteristics. In a comparison of the biochemical data between the Meg1 Tg mouse and other 2DM model mice, such as KK-A^y and BKS mouse, the Meg1 Tg mouse did not show plasma insulin and a remarkable rise of plasma glucose levels like KK-A^y and BKS mice, but showed a property that is characteristic of human 2DM, a rise of adiponectin level [5, 16, 18]. In addition, it is a very unique characteristic that this property is caused by environmental factors such as diet.

In mRNA expression analysis, diabetes related genes, such as *Grb10*, *Ucp1*, and *Glut4*, in the Meg1 Tg mouse were compared with 3 famous diabetes mouse models (Fig. 6). Regarding the relationship between the *Meg1/Grb10* gene and the non-obese character of the Meg1 Tg mouse, overexpression of the *Meg1/Grb10* gene may hold the IGF-1 acceptor signal transduction system in check during development in the embryonic stage and the holding effect would be maintained until long after birth [31]. It is reported that maternal duplication of proximal chromosome 11 retards embryonic growth, whereas paternal duplication promotes growth [2]. A recent *Grb10* knockout study has clearly demonstrated that *Meg1/Grb10* is the gene responsible for embryonic overgrowth observed in paternal duplication of the chromosome 11 region [3], although the effect of *Meg1/Grb10* overproduction remains to be addressed. Our data may provide answers to these puzzling issues. Grb10 regulates the insulin signaling and sensitivity *in vivo* [36]. This suggests that a high level of the *Grb10* gene could affect insulin resistance in the Meg1 Tg mouse. The reduction in intracellular lipid by constitutive expression of *Ucp1* reflects down-regulation of fat synthesis rather than up-regulation of fatty acid oxidation [32]. The down-regulation of *Ucp1* in Meg1Tg mice fed HFD could explain the non-obese character of the Meg1 Tg mouse. The quantity of expression of *Glut4* mRNA in skeletal muscle decreased significantly in Meg1 Tg mice (Fig. 6C). GLUT4 translocation can be activated by insulin, to which the Meg1 Tg mouse has resistance, and may be related to the GLUT4 decrease in skeletal muscle.

Recently, association of hGrb10 genetic variations with 2DM in Caucasian subjects has been reported [2]. There is no evidence of such a correlation in Japanese subjects. However, it has been revealed that the expression of hGrb10 was influenced by epigenetic alterations. It is important to investigate hGrb10 expression and the relationship to environmental conditions including diet in 2DM model mice.

Acknowledgment(s)

We thank Ms. Tomoko Hata and Naho Takekawa for technical assistance.

References

1. Caroline, S.F., Michael, J.P., James, B.M., Ramachandran, S.V., Yamini, S.L., and Ralph, B.D. 2006. Trends in the incidence of type 2 diabetes mellitus from the 1970s to the 1990s. *Circulation* 113: 2914–2918.
2. Cattanach, B.M., Beechey, C.V., Rasberry, C., Jones J., and Papworth, D. 1996. Time of initiation and site of action of the mouse chromosome 11 imprinting effects. *Genet. Res.* 68: 35–44.
3. Charalambous, M., Smith, F.M., Bennett, W.R., Crew, T.E., Mackenzie, F., and Ward, A. 2003. Disruption of the imprinted *Grb10* gene leads to disproportionate overgrowth by an Igf2-independent mechanism. *Proc. Natl. Acad. Sci. U.S.A.* 100: 8292–8297.
4. Chu, K.Y., Lau, T., Carlsson, P.O., and Leung, P.S. 2006. Angiotensin II type 1 receptor blockade improves beta-cell function and glucose tolerance in a mouse model of type 2 diabetes. *Diabetes* 55: 367–374.
5. Combs, T.P., Wagner, J.A., Berger, J., Doebber, T., Wang,

W.-J., Zhang, B.B., Tanen, M., Berg, A.H., O'Rahilly, S., Savage, D.B., Chatterjee, K., Weiss, S., Larson, P.J., Gottesdiener, K.M., Gertz, B.J., Charron, M.J., Scherer, P.E., and Moller, D.E. 2002. Induction of adipocyte complement-related protein of 30 kilodaltons by PPARg agonists: a potential mechanism of insulin sensitization. *Endocrinology* 143: 998–1007.

6. Cramer, K.L., Gerrald, Q.D., Nichols, C.B., Price, M.S., and Alspaugh, J.A. 2006. Transcription factor Nrg1 mediates capsule formation, stress response, and pathogenesis in Cryptococcus neoformans. *Eukaryotic Cell* 5: 1147–1156.
7. DeChhiara, T.M., Robertson, E.J., and Efstratiadis, A. 1991. Parental imprinting of the mouse insulin-like growth factor II gene. *Cell* 64: 849–859.
8. Dey, B.R., Frick, K., Lopaczynski, W., Nissley, S.P., and Furlanetto, R.W. 1996. Evidence for the direct interaction of the insulin-like growth factor I receptor with IRS-1, Shc, and Grb10. *Mol. Endocrinol.* 10: 631–641.
9. Dong, L.Q., Du, H., Porter, S.G., Kolakowski, L.F., Lee, A.V., Mandarino, L.J., Fan, J., Yee, D., Liu, F., and Mandarino, J. 1997. Cloning, chromosome localization, expression, and characterization of an *Src* homology 2 and pleckstrin homology domain-containing insulin receptor binding protein hGrb10gamma. *J. Biol. Chem.* 272: 29104–29112.
10. Floria, L., Joseph, D.T., Kaechoong, L., Gino, V.S., Argiris, E. 2001. Roles of growth hormone and insulin-like growth factor 1 in mouse postnatal growth. *Dev. Biol.* 229: 141–162.
11. Furuya, Y., Tagami, S., Hasegawa, A., Ishii, J., Hirokawa, J., Yoshimura, H., Honda, T., Sakaue, S., Aoki, K., Murakami, M., Kudo, I., and Kawakami, Y. 1999. Increased glomerular cytosolic phospholipase A2 activity of OLETF rats with early diabetes. *Exp. Clin. Endocrinol. Diabetes* 107: 299–305.
12. Hanley, A.J., Karter, A.J., Williams, K., Festa, A., D'Agostino, R.B. Jr., Wagenknecht, L.E., and Haffner, S.M. 2005. Prediction of type 2 diabetes mellitus with alternative definitions of the metabolic syndrome: the Insulin Resistance Atherosclerosis Study. *Circulation* 112: 3675–3676.
13. Hattersley, A.T. 2004. Unlocking the secrets of the pancreatic beta cell: man and mouse provide the key. *J. Clin. Invest.* 114: 314–316.
14. Horio, F., Teradaira, S., Imamura, T., Anunciado, R.V., Kobayashi, M., Namikawa, T., and Niki, I. 2005. The HND mouse, a nonobese model of type 2 diabetes mellitus with impaired insulin secretion. *Eur. J. Endocrinol.* 153: 971–979.
15. Kanauchi, M. 2003. Comparison in renal histology between Japanese obese and non-obese microalbuminuric type 2 diabetic patients. *Nephrol. Dial. Transplant.* 18: 849–850.
16. Kawasaki, F., Matsuda, M., Kanda, Y., Inoue, H., and Kaku, K. 2005. Structural and functional analysis of pancreatic islets preserved by pioglitazone in *db/db* mice. *Am. J. Physiol. Endocrinol. Metab.* 288: E510–E518.
17. Kushi, A., Sasai, H., Koizumi, H., Takeda, N., Yokoyama, M., and Nakamura, M. 2006. Obesity and mild hyperinsulinemia found in neuropeptide Y-Y1 receptor-deficient mouse. *Proc. Natl. Acad. Sci. U.S.A.* 95: 15659–15664.
18. Kuwabara, K., Murakami, K., Todo, M., Aoki, T., Asaki, T., Murai, M., and Yano, J. 2004. A novel selective peroxisome proliferator-activated receptor a agonist, 2-methyl-c-5-[4-[5-methyl-2-(4-methyphenyl)-4-oxazolyl]butyl]-1,3-dioxane-r-2-carboxylic acid(NS-220), potently decreases plasma triglyceride and glucose levels and modifies lipoprotein profiles in KK-A^y mice. *J. Pharmacol. Exp. Ther.* 309: 970–977.
19. Lewis, G.F., O'Meara, N.M., Soltys, P.A., Blackman, J.D., Iverius, P.H., Pugh, W.L., Getz, G.S., and Polonsky, K.S. 1991. Fasting hypertriglyceridemia in noninsulin-dependent diabetes mellitus is an important predictor of postprandial lipid and lipoprotein abnormalities. *J. Clin. Endocrinol. Metab.* 72: 934–944.
20. Louvi, A., Accili, D., and Efstratiadis, A. 1997. Growth-promoting interaction of IGF-II with the insulin receptor during mouse embryonic development. *Dev. Biol.* 189: 33–48.
21. Ma, D., Shield, J.P., Dean, W., Leclerc, I., Knauf, C., Burcelin, R.R., Rutter, G.A., and Kelsey, G. 2004. Impaired glucose homeostasis in transgenic mouse expressing the human transient neonatal diabetes mellitus locus, TNDM. *J. Clin. Invest.* 114: 339–348.
22. Miao, G., Ito, T., Uchikoshi, F., Tanemura, M., Kawamoto, K., Shimada, K., Nozawa, M., and Matsuda, H. 2005. Development of islet-like cell clusters after pancreas transplantation in the spontaneously diabetic Torri rat. *Am. J. Transplant.* 5: 2360–2367.
23. Miyoshi, N., Kuroiwa, Y., Kohda, T., Shitara, H., Yonekawa, H., Kawabe, T., Hasegawa, H., Barton, S.C., Surani, M.A., Kaneko-Ishino, T., and Ishino, F. 1998. Identification of the *Meg1/Grb10* imprinted gene on mouse proximal chromosome 11, a candidate for the Silver–Russell syndrome gene. *Proc. Natl. Acad. Sci. U.S.A.* 95: 1102–1107.
24. Momose, K., Nunomiya, S., Nakata, M., Yada, T., Kikuchi, M., and Yashiro, T. 2006. Immunohistochemical and electron-microscopic observation of beta-cells in pancreatic islets of spontaneously diabetic Goto-Kakizaki rats. *Med. Mol. Morphol.* 39: 146–153.
25. Morrione, A., Valentinis, B., Resnicoff, M., Xu, S., and Baserga, R. 1997. The role of m*Grb10*alpha in insulin-like growth factor I-mediated growth. *J. Biol. Chem.* 272: 26382–26387.
26. Nakae, J., Kido, Y., and Accili, D. 2001. Distinct and overlapping functions of insulin and IGF-I receptors. *Endcr. Rev.* 22: 818–835.
27. O'Neill, T. J., Rose, D.W., Pillay, T.S., Hotta, K., Olefsky, J.M., and Gustafson, T.A. 1996. Interaction of a GRB-IR splice variant (a human GRB10 homolog) with the insulin and insulin-like growth factor I receptors. Evidence for a role in mitogenic signaling. *J. Biol. Chem.* 271: 22506–22513.
28. Ohki, Y., Kishi, M., Orimo, H., and Ohkawa, T. 2004. Insulin resistance in Japanese adolescents with type 2 diabetes mellitus. *J. Nippon Med. Sch.* 71: 88–91.
29. Paola, R.D., Ciociola, E., Boonyasrisawat, W., Nolan, D.,

Duffy, J., Miscio, G., Cisternino, C., Fini, G., Tassi, V., Doria, A., and Trischitta, V. 2006. Association of hGrb 10 genetic variations with type 2 diabetes in Caucasian subjects. *Diabetes Care* 29: 1181–1182.

30. Reynisdottir, I., Thorleifsson, G., Benediktsson, R., Sigurdsson, G., Emilsson, V., Einarsdottir, A.S., Hjorleifsdottir, E.E., Orlygsdottir, G.T., Bjornsdottir, G.T., Saemundsdottir, J., Halldorsson, S., Hrafnkelsdottir, S., Sigurjonsdottir, S.B., Steinsdottir, S., Martin, M., Kochan, J.P., Rhees, B.K., Grant, S.F., Frigge, M.L., Kong, A., Gudnason, V., Stefansson, K., and Gulcher, J.R. 2003. Localization of a susceptibility gene for type 2 diabetes to chromosome 5q34-q35.2. *Am. J. Hum. Genet.* 73: 323–335.
31. Shiura, H., Miyoshi, N., Konishi, A., Wakisaka-Saito, N., Suzuki, R., Muguruma, K., Kohda, T., Wakana, S., Yokoyama, M., Ishino, F., and Kaneko-Ishino, T. 2005. *Meg1/Grb10* overexpression causes postnatal growth retardation and insulin resistance via negative modulation of the IGF1R and IR cascades. *Biochem. Biophys. Res. Commun.* 329: 909–916.
32. Si, Y., Palani, S., Jayaraman, A., and Lee, K. 2007. Effects of forced uncoupling protein 1 expression in 3T3-L1 cells on mitochondrial function and lipid metabolism. *J. Lipid Res.* 48: 826–836.
33. Takada, Y., Takata, Y., Iwanishi, M., Imamura, T., Sawa, T., Morioka, H., Ishihara, H., Ishiki, M., Usui, I., Temaru, R., Urakaze, M., Satoh, Y., Inami, T., Tsuda, S., and Kobayashi, M. 1996. Effect of glimepiride (HOE 490) on insulin receptors of skeletal muscles from genetically diabetic KK-A^y mouse. *Eur. J. Pharmacol.* 308: 205–210.
34. Takeuchi, M., Itakura, A., Okada, M., Mizutan, S., and Kikkawa, F. 2006. Impaired insulin-regulated membrane aminopeptidase translocation to the plasma membrane in adipocytes of Otsuka Long Evans Tokushima Fatty rats. *Nagoya J. Med. Sci.* 68: 155–163.
35. Teixeira, S.R., Tappenden, K.A., and Erdman, J.W. Jr. 2003. Altering dietary protein type and quantity reduces urinary albumin excretion without affecting plasma glucose concentrations in BKS.Cg-+$Lepr^{db}$/+$Lepr^{db}$ (*db/db*) mouse. *J. Nutr.* 133: 673–678.
36. Wang, L., Balas, B., Christ-Roberts, C.Y., Kim, R.Y., Ramos, F.J., Kikani, C.K., Li, C., Deng, C., Reyna, S., Musi, N., Dong, L.Q., DeFronzo, R.A., Liu, F. 2007. Peripheral disruption of the *Grb10* gene enhances insulin signaling and sensitivity *in vivo*. *Mol. Cell. Biol.* 27: 6497–6505.
37. Wright, N.M., Metzger, D.L., Borowitz, S.M., and Clarke, W.L. 1993. Permanet neonatal diabetes mellitus and pancreatic agenesis. *Am. J. Dis. Child.* 147: 607–609.
38. Yi, L.Z., He, J., Liang, Y.Z., Yuan, D.L., and Chau, F.T. 2006. Plasma fatty acid metabolic profiling and biomarkers of type 2 diabetes mellitus based on GC/MS and PLS-LDA. *FEBS Lett.* 580: 6837–6845.
39. 1999–2001 National Health Interview Survey and 1999–2000 National Health and Nutrition Examination Survey estimates projected to year 2002. National Diabetes Fact Sheet, National Estimates on Diabetes. CDC publications and products.